International Journal of Nanomedicine

Dovepress
open access to scientific and medical research

Open Access Full Text Article

ORIGINAL RESEARCH

Aptamer-Functionalized Dendrimer Delivery of Plasmid-Encoding lncRNA *MEG3* Enhances Gene Therapy in Castration-Resistant Prostate Cancer

This article was published in the following Dove Press journal:
International Journal of Nanomedicine

Zongguang Tai[1,2,*]
Jinyuan Ma[1,*]
Jianing Ding[1,*]
Huijun Pan[1]
Rongrong Chai[1]
Congcong Zhu[1]
Zhen Cui[1]
Zhongjian Chen[1]
Quangang Zhu[1]

[1]Shanghai Skin Disease Hospital, Tongji University School of Medicine, Shanghai 200443, People's Republic of China; [2]Department of Pharmacy, Changhai Hospital, Second Military Medical University, Shanghai 200433, People's Republic of China

*These authors contributed equally to this work

Correspondence: Quangang Zhu; Zhongjian Chen
Shanghai Skin Disease Hospital, Tongji University School of Medicine, Baode Road 1278, Shanghai 200443, People's Republic of China
Tel +86 21 61833155; +86 21 61833007
Fax +86 21 61833021
Email qgzhu@126.com; aajian818@163.com

Purpose: The clinical management of patients with castration-resistant prostate cancer (CRPC) is difficult. However, novel treatment methods are gradually being introduced. Considering the adverse effects of traditional treatments, recent studies have investigated gene therapy as a method to combat CRPC; but, the application of long non-coding (lnc) RNA in gene therapy remains scarce, despite their promise. Therefore, it is imperative to develop a system that can efficiently deliver lncRNA for the treatment of CRPC. Here, we investigated the efficacy of a delivery system by introducing the plasmid-encoding tumor suppressor lncRNA *MEG3* (pMEG3) in CRPC cells.

Materials and Methods: An EpDT3 aptamer-linked poly(amidoamine) (PAMAM) dendrimer targeting EpCAM was used to deliver pMEG3 in CRPC cells. The PAMAM-PEG-EpDT3/pMEG3 nanoparticles (NPs) were tested using in vitro cellular assays including cellular uptake, entry, and CCK-8 measurement, and tumor growth inhibition, histological assessment, and safety evaluations in in vivo animal models.

Results: The EpDT3 aptamer promoted endocytosis of PAMAM and PAMAM-PEG-EpDT3/pMEG3 NPs in CRPC cells. PAMAM-PEG-EpDT3/pMEG3 NPs exhibited a significant anti-CRPC effect, both in vivo and in vitro, when compared to that of unfunctionalized PAMAM-PEG/pMEG3 NPs.

Conclusion: PAMAM-PEG-EpDT3/pMEG3 NPs can potentially improve gene therapy in CRPC cells.

Keywords: long non-coding RNA MEG3, castration-resistant prostate cancer, gene therapy, dendrimer

Introduction

Prostate cancer (PCa) is the most common malignancy of the prostatic epithelium. It can greatly reduce the lifespan and life quality of afflicted patients. Surgical excision, radiation therapy, hormonal therapy, and chemotherapy are the primary methods for treating PCa.[1,2] However, patients may develop severe complications, iatrogenic injury, drug toxicity, and therapy resistance.[3,4]

Castration-resistant PCa (CRPC) is considered the terminal stage of the disease,[5] and prolonging the occurrence of castration-resistant malignancy remains therapeutically challenging. Gene therapy has been deployed to deliver specific nucleotide sequences to target cells, where they can correct or compensate for the

submit your manuscript | www.dovepress.com
DovePress
http://doi.org/10.2147/IJN.S282107

existing gene defect or abnormality that leads to specific diseases or inhibit the expression of oncoproteins.[6,7] Therefore, gene therapy can improve treatment with fewer adverse effects in patients with PCa.

Non-coding RNA is a general term used to describe functional RNAs that cannot encode or translate proteins. They include long non-coding RNAs (lncRNAs) and short non-coding RNAs (such as small interfering RNA and microRNA). Non-coding RNAs play a major role in chromosome transcription and inactivation, gene expression and shutdown, cell cycle regulation, and apoptosis.[8] Currently, the use of short non-coding RNAs in gene therapy studies is preferred for the treatment of various cancers.[9] However, recent studies have found lncRNAs to be closely associated with tumor development.[10] Of these, lncRNA *MEG3* is expressed in most of the normal tissues, but is scarcely detected in human tumor cells; thus, it is speculated that lncRNA *MEG3* inhibits tumor growth through ectopic expression.[11] Further, lncRNA *MEG3* was found to inhibit DNA synthesis by stimulating p53-mediated transcription, thereby inhibiting proliferation in meningioma cells.[12,13] Luo et al also showed that lncRNA *MEG3* inhibits proliferation and induces apoptosis by upregulating the expression of p53 in CRPC cells.[14] Therefore, lncRNA *MEG3* is a promising tumor suppressor that may have clinical applications in the treatment of CRPC.

Several studies have investigated the mechanism of action of lncRNAs, including their anticancer roles.[15] However, only a few lncRNAs are identified that exert tumor suppressor functionality. Moreover, they are difficult to synthesize owing to their length and poor stability.[10,16,17] Therefore, we constructed the plasmid-encoding lncRNA *MEG3* (pMEG3) to overcome the lncRNA instability. Given the lack of suitable vectors, the ability to deliver lncRNAs into tumor cells through nano-drug delivery systems in vivo, including to PCa cells, has become a focus of translational medicine research.

EpCAM (also known as TACSD1 and CD326) is a glycoprotein highly expressed on the surfaces of a majority of malignant epithelial tumor cells. EpCAM is one of the most strongly expressed tumor surface antigens that promotes cell proliferation, differentiation, and migration, cell cycle acceleration, immune escape, and other biological functions.[18,19] Other studies have found that EpCAM is associated with resistance to radiation and chemotherapy, and metastasis of PCa cells via activation of the PI3/Akt/mTOR signaling pathway.[20] EpCAM is highly expressed on the PCa cells of patients with carcinoma in situ and lymph node metastasis, especially in those with CRPC (including in >80% of circulating PCa cells).[21,22] This renders the protein a promising coupling molecule for use with antibodies or other molecules targeting PCa cells.

Aptamers are single-stranded RNA or DNA molecules that form hairpin and additional secondary structures determined by specific sequences to achieve target recognition.[23,24] Furthermore, a host of aptamers selected and generated from large synthetic libraries through the "systemic evolution of ligands by exponential enrichment (SELEX)" technique are optimal candidates for drug delivery, given their binding to specific targets.[25] Shigdar et al developed a 19-nt RNA aptamer (EpDT3) that specifically binds to cancer cells that overexpress EpCAM on the cell surface and are endocytosed after binding to the molecule.[26,27] The aptamer can further target EpCAM-overexpressing PCa cells by modifying specific drug or gene carriers, thereby effectively repressing PCa.

Poly(amidoamine) (PAMAM) dendrimers are the earliest and most widely used polymers; they have layered three-dimensional structures and are extensively used for medical applications. The surface groups on PAMAM can be used as anchor points that bind or absorb different types of reagents to achieve various functions, such as improving targeting capability, modifying solution behavior, and reducing toxicity.[28,29] In our current study, EpDT3 and polyethylene glycol (PEG) were attached to the surface of PAMAM to develop a new vector—PAMAM-PEG-EpDT3— to deliver pMEG3 to CRPC cells. CRPC cell lines and xenograft mouse models were used to evaluate the targeting ability and mechanism of cellular uptake of PAMAM-PEG-EpDT3, as well as the therapeutic effect of PAMAM-PEG-EpDT3/pMEG3 nanoparticles (NPs) loaded with pMEG3 (Figure 1).

Materials and Methods

Materials

Analytical grade chemical reagents were purchased from Shanghai Lingfeng Chemical Reagent Co., Ltd (Shanghai, China). Deionized water was used for all experiments unless otherwise stated. Maleimide PEG3500 succinimidyl carboxymethyl ester (NHS-PEG-MAL, MW 3500) was purchased from JenKem Technology Co., Ltd (Beijing, China). Furthermore, pMEG3, Lipofectamine 2000, and BODIPY-493/503 NHS ester were obtained from Life

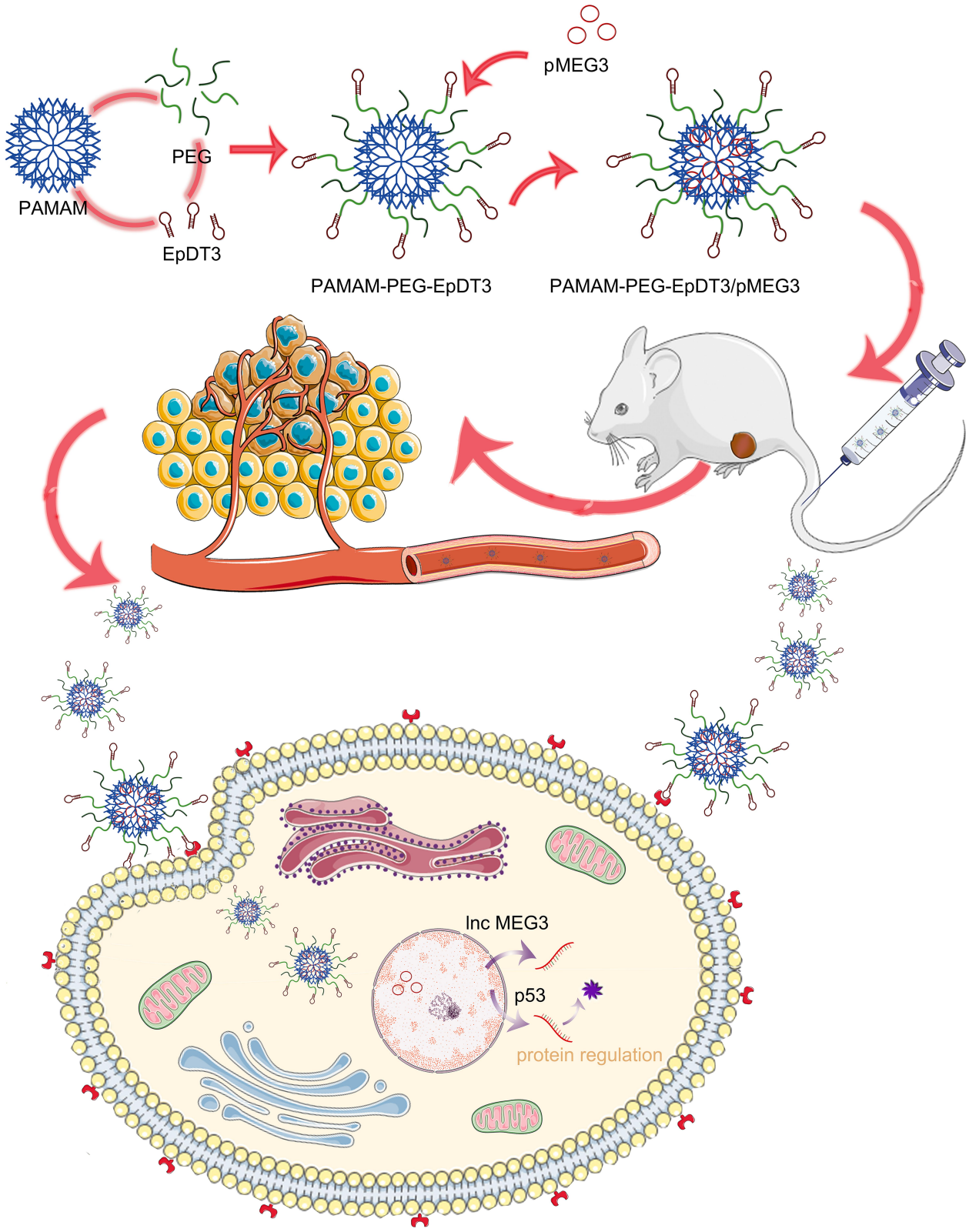

Figure 1 Schematic illustration of using PAMAM-PEG-EpDT3/pMEG3 nanoparticles to target castration-resistant prostate cancer cells.
Abbreviations: lncRNA, long non-coding RNA; PAMAM, poly(amidoamine); PEG, polyethylene glycol; pMEG3, plasmid-encoding lncRNA *MEG3*.

Technologies (Carlsbad, CA, USA). Control pDNA was purchased from Invitrogen (Thermo Fisher Scientific Inc., Carlsbad, CA, USA). Ethidium monoazide bromide (EMA) was obtained from Shanghai Aladdin Co., Ltd (Shanghai China). PAMAM dendrimer G5 was purchased from Sigma-Aldrich (St Louis, MO, USA). Aptamer EpDT3 and Cy3 fluorescein-labeled EpDT3 with 5′-thiolation were synthesized by Guangzhou RiboBio Co., Ltd (Guangzhou, China), as described previously.[26] The sequence of EpDT3 is 5′/5thiol/-GCGACUGGUUACCCGGUCG-3′.

Cell Culture

PC-3 and DU-145 CRPC cell lines were obtained from the Chinese Academy of Sciences (Shanghai, China). The cells were cultured in RPMI 1640 medium containing 10% fetal bovine serum, 100 μg/mL streptomycin, and 100 U/mL penicillin in a 5% CO_2 humidified incubator at 37°C.

Synthesis of PAMAM-PEG-EpDT3

PAMAM G5 was solubilized in methyl alcohol, followed by drying with nitrogen. The PEG with two functional groups (NHS-PEG-MAL) was diluted in phosphate-buffered saline (PBS; pH 8.0) to 10 mg/mL. The PAMAM and NHS-PEG-MAL (molar ratio of 1:2) were stirred at room temperature for 2 h in the dark. The resulting mixture was concentrated twice by an ultrafiltration device (molecular weight cut-off: 10 kDa) at 12,000 rpm for 20 min at 4°C and resolubilized in PBS (pH 7.0). The final product was lyophilized to obtain PAMAM-PEG-MAL.

The thiolated EpDT3 was coupled to the MAL component of the synthesized PAMAM-PEG-MAL. Briefly, the PAMAM-PEG-MAL mixture and thiolated EpDT3 (molar ratio of 10:1) were stirred in a nitrogen-rich atmosphere at room temperature for 24 h in the dark. Further purification was performed by ultrafiltration (5000 g, 15 min) to obtain PAMAM-PEG-EpDT3. The resulting synthesized product was identified by proton nuclear magnetic resonance (^{1}H-NMR) analysis on a Varian Mercury Plus NMR 400 MHz spectrometer (Varian, Salt Lake City, UT, USA).

To obtain a BODIPY-labeled PAMAM-PEG-EpDT3, BODIPY-493/503 NHS ester and PAMAM-PEG-EpDT3 (molar ratio of 5:1) were mixed in $NaHCO_3$ working solution (100 mM) and stirred at 4°C in the dark for 12 h. Subsequently, the unreacted BODIPY was removed using an ultrafiltration device (MWCO 10,000) at 12,000 rpm for 20 min at 4°C. Next, the end-product (BODIPY-PAMAM-PEG-EpDT3) was collected and lyophilized.

Evaluation of Cellular Uptake of PAMAM-PEG-EpDT3

To evaluate the binding capacity of EpDT3 to CRPC cells, PC-3 and DU-145 cells were seeded onto chambered coverslips in 24-well plates at a density of 7×10^4/mL and cultured to 50% confluence before the culture medium was removed. Cy3-EpDT3 at a concentration of 100 nM was added for 30 minutes to evaluate the localization of EpDT3; untreated cells were used as blank controls. Subsequently, the culture medium was removed, and the cells were fixed in 4% paraformaldehyde for 20 min. Next, the nuclei were stained with bisbenzimide Hoechst 33,342 (3 μg/mL) for 15 min. Finally, the cells were washed, and the intracellular location of EpDT3 was captured using a Leica SP8 inverted confocal microscope (Leica, Heidelberg, Germany) under ×100 magnification.

Fluorescence microscopy was used to evaluate the uptake of PAMAM-PEG-EpDT3 by PC-3 and DU-145 cells in a concentration-dependent manner. The cells were seeded in 24-well plates at a density of 7×10^4/mL and cultured to 90% confluence. Further, BODIPY-PAMAM-PEG-EpDT3 at PAMAM concentrations of 0.05, 0.1, 0.2, 0.5, and 1 μM was added to the culture medium. The cells were incubated for 30 min, washed three times with PBS, and observed with an IX53 inverted fluorescence microscope (Olympus, Tokyo, Japan) to evaluate the cellular uptake of PAMAM-PEG-EpDT3.

Flow cytometry was also used to study the uptake of PAMAM-PEG-EpDT3 into PC-3 and DU-145 cells. The cells were seeded in 6-well plates at a density of 2×10^5/mL and cultured to 90% confluence. Further, BODIPY-PAMAM-PEG-EpDT3, BODIPY-PAMAM-PEG, or BODIPY-PAMAM was added to the culture medium at a concentration of 0.5 μM. After incubation for 30 min, the cells were washed, trypsinized, and resuspended in 200 μL PBS (pH 7.0). The fluorescence intensity of BODIPY was measured using a flow cytometer (NovoCyte, ACEA Biosciences Inc., Hangzhou, China) to determine the cellular uptake. Untreated cells were used as negative controls.

Preparation of PAMAM-PEG-EpDT3 /pMEG3 NPs

pMEG3 was used to construct PAMAM-PEG-EpDT3 /pMEG3 NPs to investigate their inhibitory effect on

CRPC cells. pMEG3 was diluted to 100 μg/mL with 50 mM Na_2SO_4, which was mixed with newly synthesized PAMAM, PAMAM-PEG, and PAMAM-PEG-EpDT3 at different nitrogen-to-phosphorus (N/P) ratios for 30 s and incubated at room temperature for 30 min.

Characterization of PAMAM-PEG-EpDT3 /pMEG3 NPs

The particle sizes of PAMAM/pMEG3, PAMAM-PEG /pMEG3, and PAMAM-PEG-EpDT3/pMEG3 were measured using dynamic light scattering, and the zeta potential was measured via electrophoretic light scattering with a Zetasizer Nano ZS90 particle size and zeta potential analyzer (Malvern Panalytical, Malvern, UK).

Agarose gel electrophoresis was performed to evaluate the encapsulation efficiency of PAMAM-PEG-EpDT3. Samples of PAMAM/pMEG3, PAMAM-PEG/pMEG3, and PAMAM-PEG-EpDT3/pMEG3 at N/P ratios of 1, 5, 10, 15, and 20 were resolved by agarose gel electrophoresis (0.5%) and visualized using Gelview staining. The naked pMEG3 and 1 kbp DNA ladder served as controls.

Endocytosis Inhibition Study

EMA was used to label the plasmid vector pMEG3 according to the manufacturer's protocol. To elucidate the mechanism underlying cellular uptake, PC-3 cells were seeded onto coverslips placed in 24-well plates at a density of 7×10^4/mL and cultured to 90% confluence. Endocytosis inhibitors, such as filipin (inhibitor of caveolin-mediated endocytosis), phenylarsine oxide (which inhibits clathrin-mediated endocytosis), and colchicine (which inhibits macropinocytosis) were added to the culture medium. After pre-treatment for 30 min, the cells were incubated with fresh culture medium containing BODIPY-PAMAM-PEG-EpDT3 (equivalent to 1 μM PAMAM) for an additional 30 min. To assess whether the uptake was energy-dependent, the cells were incubated with BODIPY-PAMAM-PEG-EpDT3 at 4°C for 30 min. To investigate the specificity of the cellular uptake of PAMAM-PEG-EpDT3, PC-3 cells were pretreated with 10 μM EpDT3 for 30 min to saturate the EpCAM receptor, followed by washing with PBS and examination by fluorescence microscopy.

The subsequent steps were performed as described above to investigate the cellular uptake of PAMAM-PEG-EpDT3/EMA-pMEG3.

Cytotoxicity Assays in vitro

The cytotoxicity of PAMAM, PAMAM-PEG and PAMAM-PEG-EpDT3 vehicles was investigated to determine their safety using the CCK-8 kit according to the manufacturer's instructions. PC-3 cells were seeded in 96-well plates at a density of 8×10^3/well and cultured for 24 h. The culture medium was replaced with PAMAM, PAMAM-PEG, and PAMAM-PEG-EpDT3 at concentrations of 20, 100, 200, 300, and 400 μg/mL. After incubation for 24 h, 10 μL of CCK-8 reagent was added to each well and incubated for an additional 1 h. Subsequently, the absorbance was measured at 450 nm using the SpectraMax M2 Multiskan Spectrum microplate reader (Molecular Devices, San Jose, CA, USA). Cell viability was calculated using the following formula: Survival (%) = (A450 nm of treated cells − A450 nm of blank)/(A450 nm of control cells − A450 nm of blank) × 100%, where the A450 nm represents the absorbance value. Each assay was performed six times.

The anti-CRPC effect of PAMAM-PEG-EpDT3 /pMEG3 in vitro was also determined using the CCK-8 assay as described above. PAMAM-PEG-EpDT3/pMEG3, PAMAM-PEG/pMEG3, and PAMAM/pMEG3 (N/P=15) were added to PC-3 cells at pMEG3 concentrations of 0.02, 0.05, 0.1, 0.3, 0.6, 1, 3, 9, and 30 μM. After 48 h of incubation, the CCK-8 assay was performed as described above.

In vivo Antitumor Study

BALB/c male nude mice (4-weeks old) were purchased from Shanghai SLAC Laboratory Animal Co., Ltd, and maintained in a specific pathogen-free environment. All animal experiments complied with the standard operating procedures approved by the animal ethics committee. To establish tumors, 1×10^7 PC-3 cells suspended in 200 μL PBS were subcutaneously injected into nude mice on the back of the right hind leg. The mice were used for further experimentation when their tumor volumes reached approximately 100 mm^3.

Nude mice (n=20) with PC-3 xenograft tumors of uniform shape and size were randomly divided into four groups (n=5, per group) and were treated with A) PBS, B) PAMAM-PEG-EpDT3/pDNA, C) PAMAM-PEG/pMEG3, or D) PAMAM-PEG-EpDT3/pMEG3. The injections were administered intravenously on days 1, 3, 5, 7, and 9 at a dose of 2.5 mg/kg pDNA or pMEG3, followed by observation for 10 days. The mice were weighed every 2 days.

Subsequently, the mice were sacrificed, and the tumors and vital organs were excised for analysis. Additionally, 1.5 mL of whole blood was withdrawn to measure alanine aminotransferase (ALT), aspartate aminotransferase (AST), and creatinine (CRE) levels.

Histological Analysis

Tumor tissues were fixed in 4% paraformaldehyde for 24 h. After dehydration in alcohol gradients, the tumor tissues were embedded in paraffin, sliced into 4 μm-thick sections, dewaxed, and stained with hematoxylin and eosin. Images were acquired using a Nikon Eclipse CI microscope (Tokyo, Japan) equipped with a DS-U3 imaging system for histopathological evaluation.

The expression of Ki67, Bcl-2, cyclin D1, and p53 proteins in tumor tissues was detected using immunohistochemistry by an experienced pathologist according to a previous report.[30]

Statistical Analysis

The SPSS 18.0 software was used for statistical analysis, and data are presented as mean ± standard deviation. One-way analysis of variance was used to analyze the significance between groups. A P-value <0.05 denoted a significant difference.

Results and Discussion

Preparation and Characterization of PAMAM-PEG-EpDT3/pMEG3 NPs

The purity of the commercially synthesized EpDT3 was determined to be >90% via high-pressure liquid chromatography. The molecular weights of EpDT3 and 5′Cy3-EpDT3 were found to be 6285.6 and 6853.8, respectively, using mass spectrometry (Figure 2A and B).

The steps for syntheses of PAMAM-PEG and PAMAM-PEG-EpDT3 are illustrated in Figure 2C. The characteristic PAMAM-PEG-EpDT3 group was verified by ^{1}H-NMR spectra. As shown in Figure 2D, a PAMAM skeleton peak appeared at 2.2–3.4 ppm. Moreover, the methylene characteristic absorption peak (δ 3.6) was verified on the ^{1}H-NMR spectra of PAMAM-PEG and PAMAM-PEG-EpDT3, indicating that PEG was conjugated with PAMAM. The amino group on the surface of PAMAM reacted with the succinimide of NHS-PEG-MAL, while the disappearance of the characteristic MAL peak (δ 6.7) on the ^{1}H NMR spectrum of PAMAM-PEG-EpDT3 further suggested that EpDT3 was linked to PEG. The introduction of PEG not only partially blocks the positive charge of PAMAM and reduces toxicity but also renders PAMAM-PEG a gene carrier with a prolonged circulatory effect.[31] Consequently, PAMAM-PEG-EpDT3 was formed owing to the reaction between the sulfhydryl groups of the EpDT3 and MAL on one end of the PEG chain (Figure 2C). As MAL and SH react under mild conditions, the EpDT3 activity was maintained during synthesis of PAMAM-PEG-EpDT3.

Newly prepared PAMAM, PAMAM-PEG, and PAMAM-PEG-EpDT3 were incubated with varying amounts of pMEG3 to formulate the pMEG3-loaded NPs. Agarose gel electrophoresis was used to evaluate the binding ability of pDNA. As shown in Figure 3A, the vehicles encapsulate pMEG3 without any leakage when the N/P ratio is > 10. Next, we selected PAMAM-PEG-EpDT3 /pMEG3 NPs prepared at an N/P ratio of 15 for further evaluation. The mean particle size of PAMAM-PEG-EpDT3/pMEG3 NPs is 180±0.15 nm with a polydispersity of 0.236 and zeta potential 19.7±0.23 mV (Figure 3B and C). The appropriate particle size and zeta potential ensure that the NPs are enriched in tumor tissues through the enhanced permeability and retention effect, and are thus taken up by tumor cells.[32,33] The mean particle size of PAMAM/pMEG3 and PAMAM-PEG/pMEG3 NPs were 141.9 nm and 158.6 nm, respectively. Moreover, we found that the PEG and EpDT3 connection increased the particle size of dendrimer/pMEG3 NPs (Figure 3A). However, PEG and EpDT3 had little effect on the potential of dendrimer/pMEG3 NPs (Figure 3C).

Evaluation of the Targeting Ability of EpDT3 and PAMAM-PEG-EpDT3

PC-3 and DU-145 cells expressing EpCAM were used as in vitro CRPC cell models. Shigdar et al suggested that the aptamer EpDT3 binds specifically to EpCAM expressed on the surface of CRPC cells and mediates endocytosis.[21,22] The localization of EpDT3 was investigated using confocal laser scanning microscopy. As shown in Figure 4A, the Cy3-EpDT3 signals in PC-3 and DU-145 cells are distributed both in the cytoplasm and membranes, suggesting that EpDT3 is successfully internalized by CRPC cells.

The selective and effective uptake of nanomaterials by target cells confers a therapeutic effect,[34,35] thus, EpDT3 can be hypothesized to increase the uptake of nanomaterials in CRPC cells. To further investigate the uptake mechanism, we first loaded the commercially available fluorescent probe BODIPY onto PAMAM-PEG-EpDT3, and then incubated

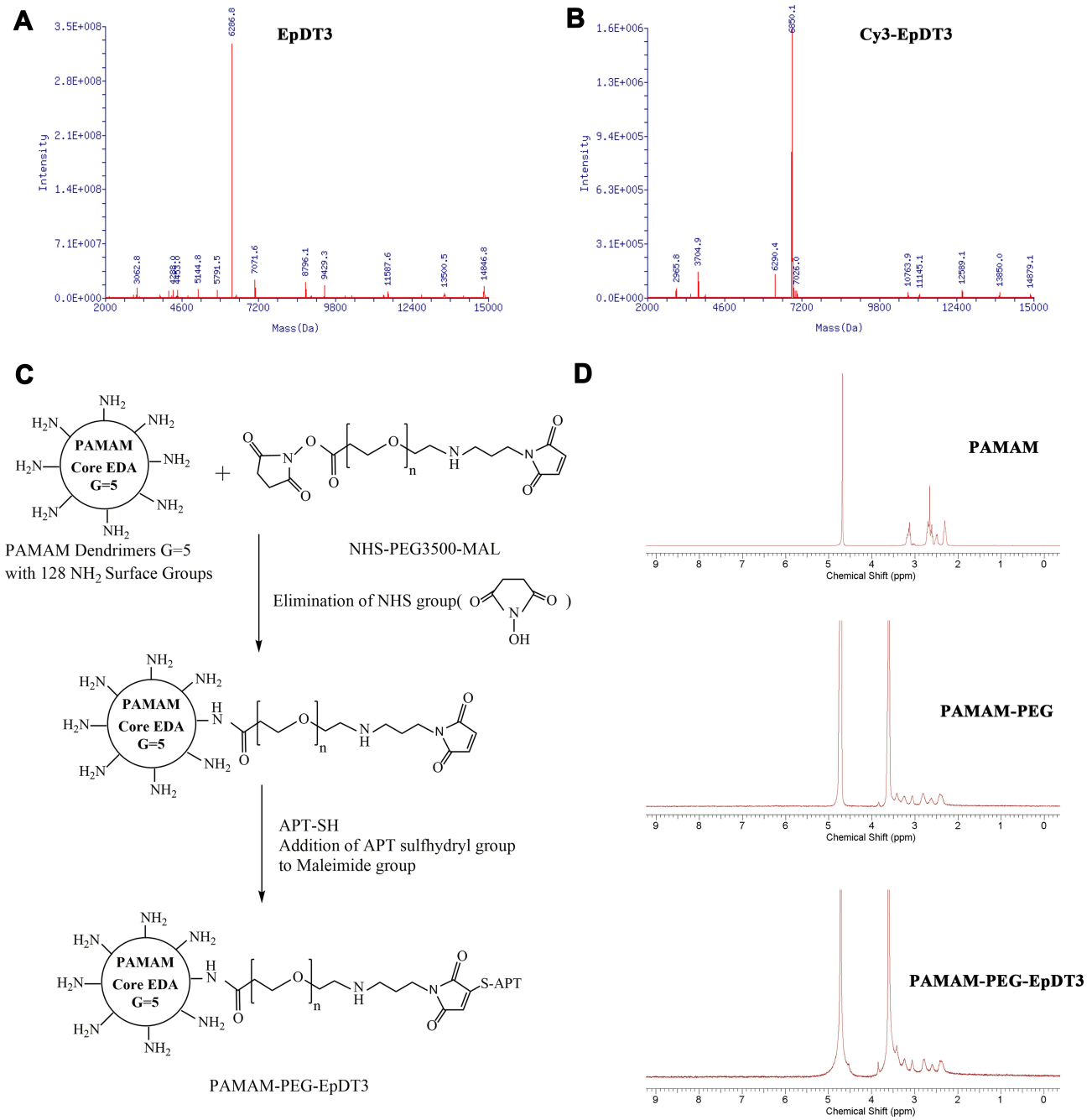

Figure 2 Synthesis and characterization of PAMAM-PEG-EpDT3. Mass spectrometry report of (**A**) thiol-EpDT3 and (**B**) Cy3-EpDT3. (**C**) Synthesis of PAMAM-PEG-EpDT3. (**D**) Proton nuclear magnetic resonance spectra of PAMAM, PEG, PAMAM-PEG, and PAMAM-PEG-EpDT3.
Abbreviations: NHS, N-hydroxysuccinimide; PAMAM, poly(amidoamine); PEG, polyethylene glycol; pMEG3, plasmid-encoding long non-coding RNA *MEG3*.

the resultant BODIPY-PAMAM-PEG-EpDT3 with PC-3 and DU-145 cells at various concentrations; its uptake is evaluated qualitatively (Figure 4B). The BODIPY signal increased in a concentration-dependent manner, indicating that EpDT3 increases the cellular uptake of PAMAM. When the concentration of BODIPY-PAMAM-PEG-EpDT3 was 0.05–1 μM, the uptake in PC-3 and DU-145 cells positively correlated with the concentration of the vehicle.

Quantitative analysis via flow cytometry also revealed that the cellular uptake of BODIPY-PAMAM-PEG-EpDT3 increased compared to that of BODIPY-PAMAM-PEG and BODIPY-PAMAM; BODIPY fluorescence in PC-3 cells increased from 77.97% to 92.14%, while that in DU-145 cells increased from 64.68% to 97.22%. The cellular uptake of PAMAM-PEG-EpDT3 is higher than that of PAMAM-PEG, indicating binding of EpDT3 to CRPC

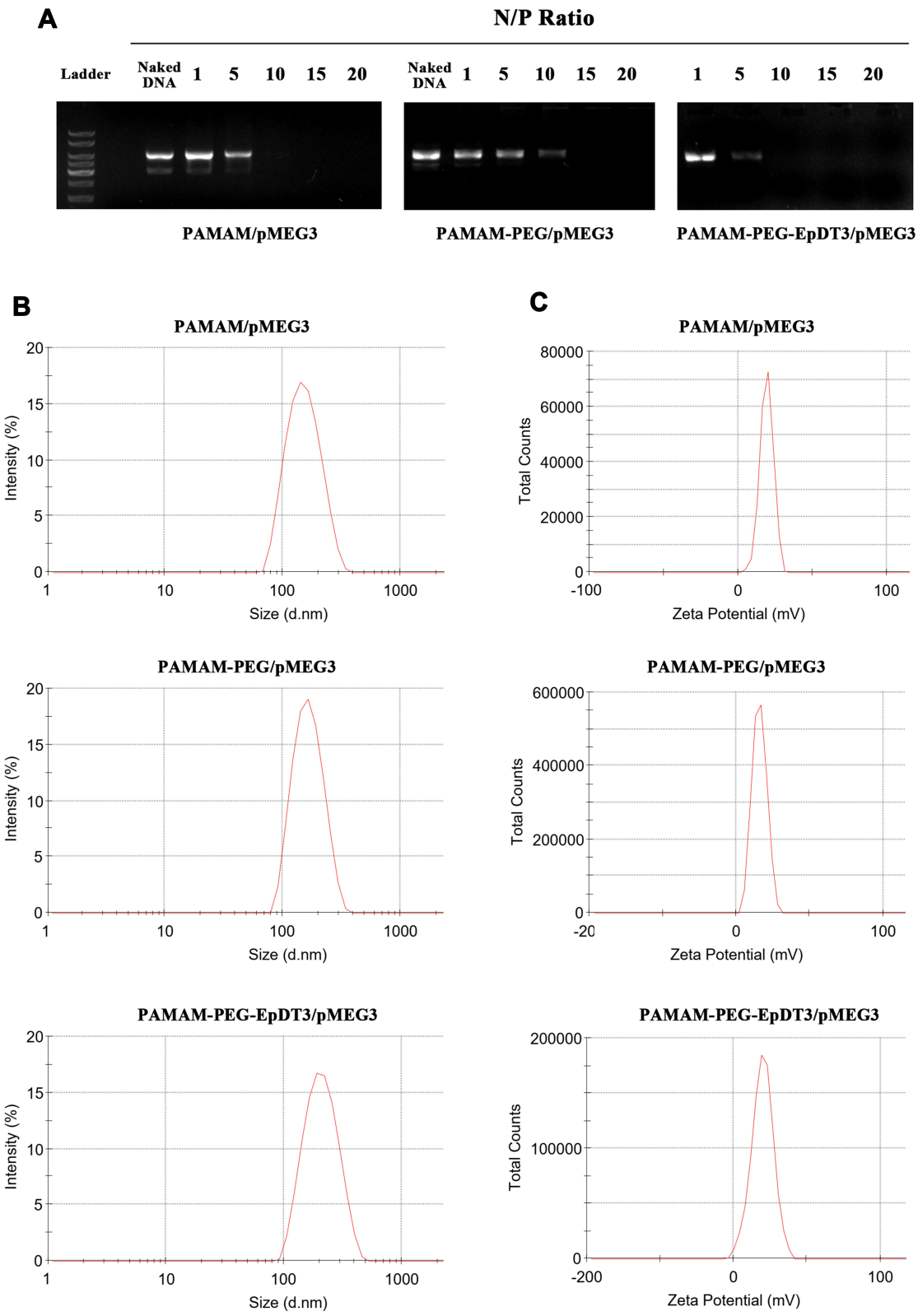

Figure 3 Characterization of complexes formed by dendrimer and pMEG3. (**A**) Agarose gel electrophoresis assay for PAMAM/pMEG3, PAMAM-PEG/pMEG3, and PAMAM-PEG-EpDT3/pMEG3 complexes at different N/P ratios. (**B**) Size distribution of PAMAM/pMEG3, PAMAM-PEG/pMEG3, and PAMAM-PEG-EpDT3/pMEG3 complexes at N/P=15 as estimated by dynamic light scattering. (**C**) Zeta potential distribution of PAMAM/pMEG3, PAMAM-PEG/pMEG3, and PAMAM-PEG-EpDT3/pMEG3 complexes at N/P=15 via electrophoretic light scattering.

Abbreviations: N/P ratio, nitrogen-to-phosphorous ratio; PAMAM, poly(amidoamine); PEG, polyethylene glycol; pMEG3, plasmid-encoding long non-coding RNA *MEG3*.

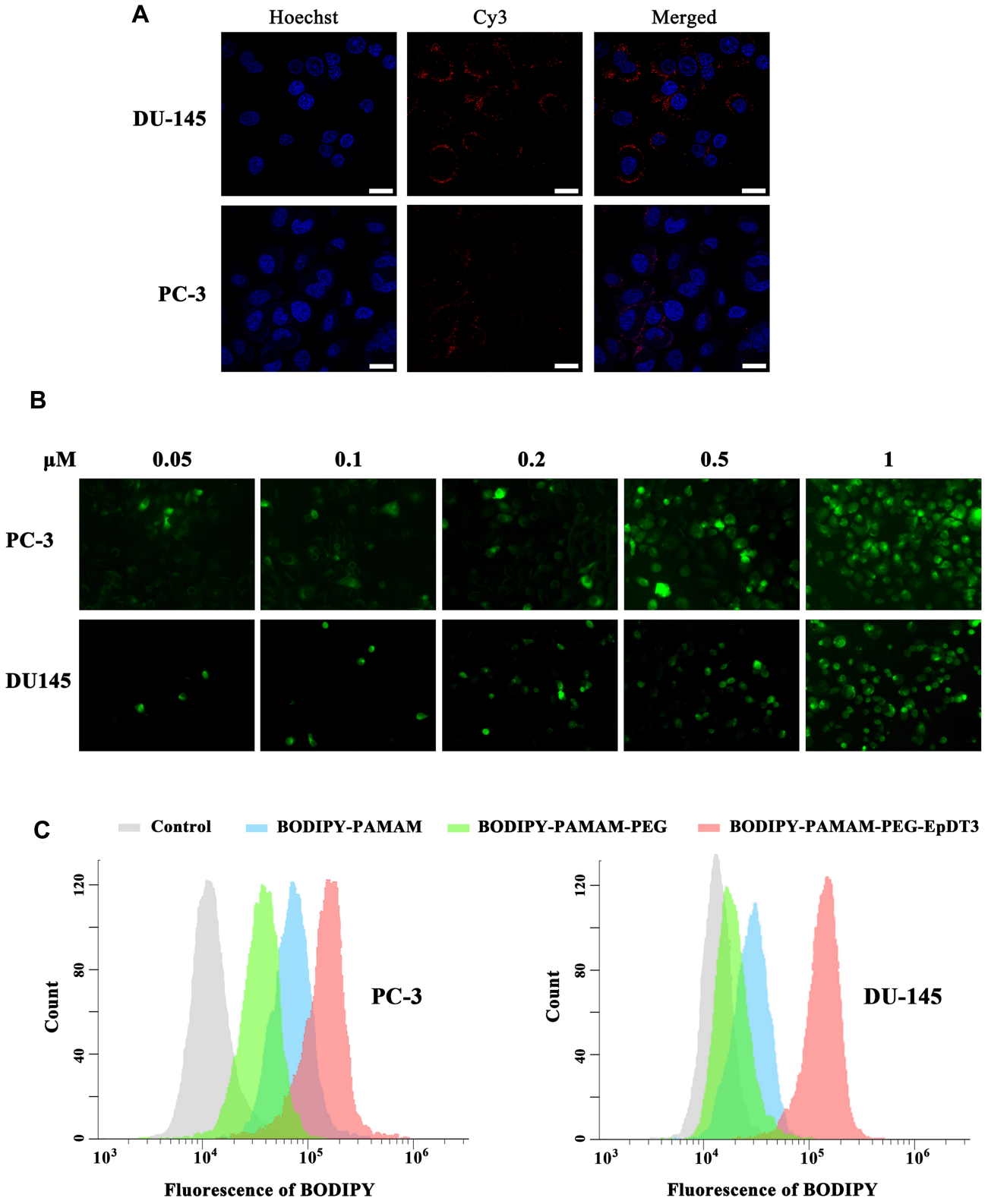

Figure 4 Evaluation of the targeting ability of EpDT3 and PAMAM-PEG-EpDT3. (**A**) Evaluation of Cy3-EpDT3 targeting PC-3 and DU-145 cells. Blue: Hoechst, Red: Cy3-EpDT3. Scale bar represents 25 μm. (**B**) Cellular uptake of BODIPY-PAMAM-PEG-EpDT3 at concentrations of 0.05, 0.1, 0.2, 0.5, and 1 μM in PC-3 and DU-145 cells after 30 min incubation. Original magnification: ×100. (**C**) BODIPY-positive PC-3 and DU-145 cells detected by flow cytometry after treatment with BODIPY-PAMAM, BODIPY-PAMAM-PEG, and BODIPY-PAMAM-PEG-EpDT3.

Abbreviations: PAMAM, poly(amidoamine); PEG, polyethylene glycol; pMEG3, plasmid-encoding long non-coding RNA *MEG3*.

cells (Figure 4C). These results were similar to observations under a confocal laser scanning microscope.

Endocytosis Mechanism Study

Next, we examined the mechanism of BODIPY-PAMAM-PEG-EpDT3 endocytosis in PC-3 cells. As shown in Figure 5A, the green fluorescence intensity in each group declined after treatment with endocytosis inhibitors. Compared to the control group, the fluorescence intensity was significantly decreased in filipin- and phenylarsine oxide-treated groups, while colchicine had a lower influence on cellular uptake. When BODIPY-PAMAM-PEG-EpDT3 was incubated with cells at 4°C, the cellular uptake of the vehicle was reduced significantly, indicating that the endocytosis of BODIPY-PAMAM-PEG-EpDT3 occurred through an energy-dependent pathway.

We investigated the mechanism of the cellular uptake of PAMAM-PEG-EpDT3/pMEG3 by PC-3 cells (Figure 5B). Interestingly, a decrease in the red fluorescence intensity of EMA was observed in all endocytosis inhibitor-treated cells. Moreover, endocytosis of EpDT3-, filipin-, and phenylarsine oxide-treated cells was decreased with lower red fluorescence intensity than in control cells, although the decrease in intensity in the colchicine-treated group was not significant. Thus, it can be deduced that this process was energy-dependent. Additionally, the endocytosis mediated by EpCAM and EpDT3, as well as the electrostatic interaction between the cationic surface of PAMAM-PEG-EpDT3 and cell membrane may also mediate endocytosis. After treating with excessive EpDT3 to compete with the complex, the cellular uptake of PAMAM-PEG-EpDT3/EMA-DNA declined markedly, suggesting that EpDT3 specifically binds to the cell membrane and enhances the cellular uptake of PAMAM-PEG-EpDT3/pMEG3.

In vitro PCa Cell Line Toxicity

PAMAM, PAMAM-PEG, and PAMAM-PEG-EpDT3 empty vectors were incubated with PC-3 and DU-145 cells, and their effects and potential toxicity were studied using CCK-8 assays. The viability of PAMAM-treated cells was significantly lower than that of PAMAM-PEG or PAMAM-PEG-EpDT3-treated cells at the same concentration, indicating that the modification of PEG and EpDT3 markedly reduces the toxicity of PAMAM, thereby improving the biocompatibility of the NPs (Figure 6A and B).

According to previous studies,[14] the expression of lncRNA *MEG3* in PCa tissues is significantly lower than that in adjacent normal prostate tissues; lncRNA *MEG3* inhibits tumor cell proliferation or induces apoptosis by stimulating p53-dependent transcription. Therefore, we constructed plasmid expressing lncRNA *MEG3* (pMEG3) and PAMAM-PEG-EpDT3/pMEG3 NPs to study their effect on CRPC cells using CCK-8 assays. PAMAM-PEG-EpDT3/pMEG3, PAMAM-PEG/pMEG3, and PAMAM/pMEG3 complexes were cytotoxic to CRPC cells in a dose-dependent manner when incubated for 48 h (Figure 6C and D). In PC-3 cells, the half-maximal inhibitory concentrations (IC_{50} values) of PAMAM-PEG-EpDT3/pMEG3, PAMAM-PEG/pMEG3, and PAMAM/pMEG3 were 2.877, 6.06, and 4.272 μM, respectively; while in DU-145 cells, the IC_{50} values of PAMAM-PEG-EpDT3/pMEG3, PAMAM-PEG/pMEG3, and PAMAM/pMEG3 were 0.695, 4.41 and 2.872 μM,

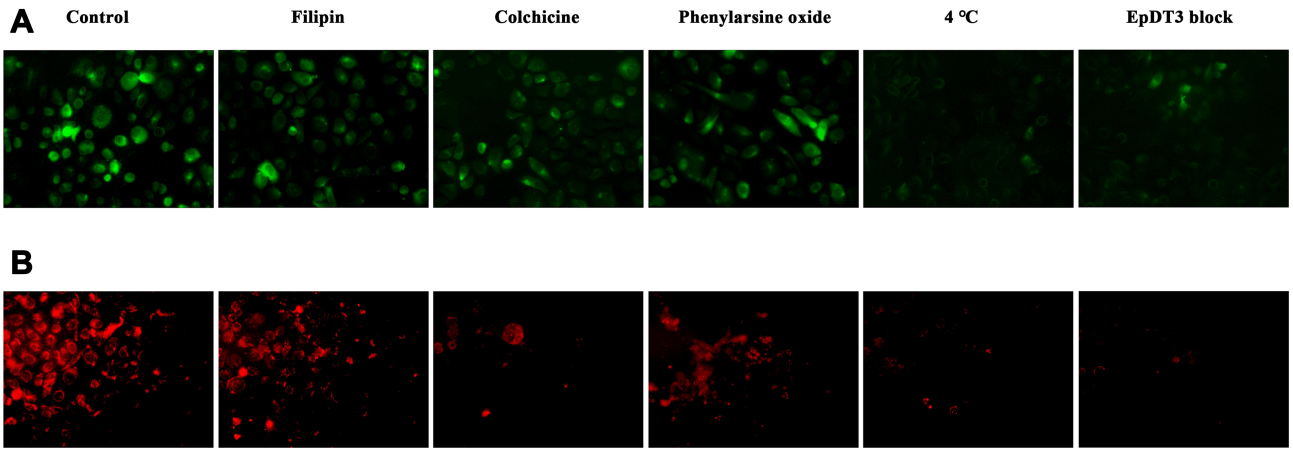

Figure 5 Endocytosis mechanism study of BODIPY-PAMAM-PEG-EpDT3 and PAMAM-PEG-EpDT3/pMEG3 NPs. (**A**) Mechanism of endocytosis of BODIPY-PAMAM-PEG-EpDT3 in PC-3 cells. Green fluorescence: BODIPY. Original magnification: ×100. (**B**) Mechanism of endocytosis of PAMAM-PEG-EpDT3/pMEG3 in PC-3 cells. Red fluorescence: Ethidium monoazide bromide-pMEG3. Original magnification: ×100.

Abbreviations: PAMAM, poly(amidoamine); PEG, polyethylene glycol; pMEG3, plasmid-encoding long non-coding RNA *MEG3*.

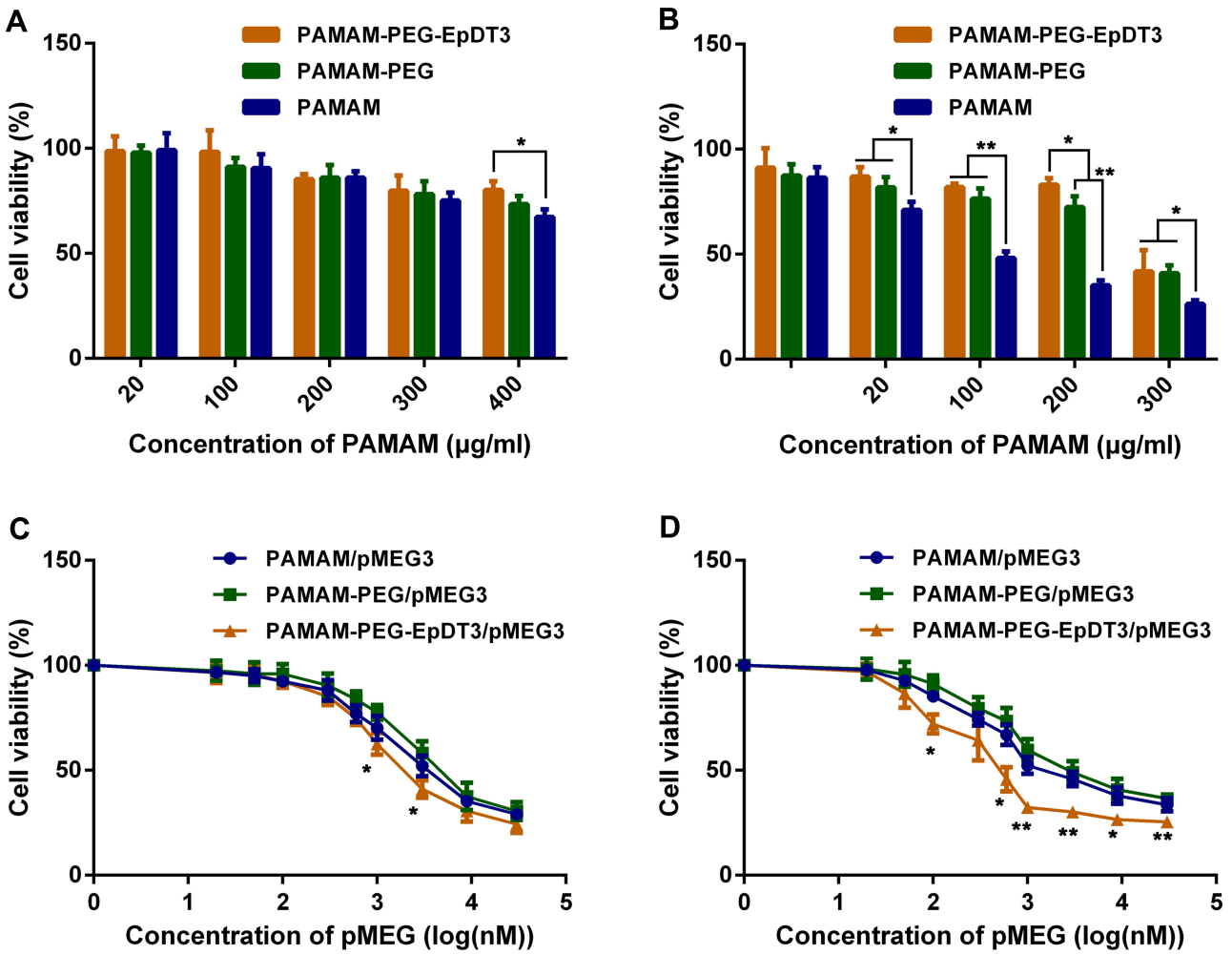

Figure 6 Anti-CRPC effect in vitro determined by CCK-8 assay. Cell viability of (**A**) PC-3 and (**B**) DU-145 cells incubated with PAMAM, PAMAM-PEG, and PAMAM-PEG-EpDT3 for 4 h. Cell viability of (**C**) PC-3 and (**D**) DU-145 cells treated with PAMAM-PEG-EpDT3/pMEG3, PAMAM-PEG/pMEG3, and PAMAM/pMEG3 complexes for 48 h. Data represent mean ± standard deviation (n=6). *P<0.05, **P<0.01.
Abbreviations: PAMAM, poly(amidoamine); PEG, polyethylene glycol; pMEG3, plasmid-encoding long non-coding RNA *MEG3*.

respectively. This indicated that PAMAM-PEG-EpDT3 /pMEG3 was more potent than PAMAM-PEG/pMEG3, which may be attributable to the increased aptamer-mediated cell uptake.

In vivo Anticancer Efficacy and Safety Evaluation

Nude mice were subcutaneously injected with PC-3 cells to establish a CRPC animal model to test the anti-CRPC efficacy of PAMAM-PEG-EpDT3/pMEG3 NPs. The tumor images of CRPC tumor-bearing nude mice are shown in Figure 7A. The tumor volume in the saline control and PAMAM-PEG-EpDT3/pDNA groups was relatively large than that in PAMAM-PEG/pMEG3 group, which was larger than that in PAMAM-PEG-EpDT3/pMEG3 group. These data showed that PAMAM-PEG/pMEG3 and PAMAM-PEG-EpDT3/pMEG3 can effectively inhibit the growth of PC-3 transplanted tumors. Moreover, PAMAM-PEG-EpDT3 /pMEG3 exerted a better anticancer effect than PAMAM-PEG/pMEG3 that could be attributed to the potent tumor-targeting potential of PAMAM-PEG/pMEG3, facilitating improved entry of the NPs into tumor cells.

The weights of the tumors isolated after the experiment are shown in Figure 7B. Compared with the saline group, PAMAM-PEG-EpDT3/pDNA inhibited tumor growth by only 5.35%; as such, no obvious antitumor effect was demonstrated. However, PAMAM-PEG/pMEG3 and PAMAM-PEG-EpDT3/pMEG3 treatment inhibited CRPC tumor growth by 40.95% and 63.34%, respectively. Furthermore, PAMAM-PEG-EpDT3/pMEG3 produced a higher tumor suppression effect than other NPs. These

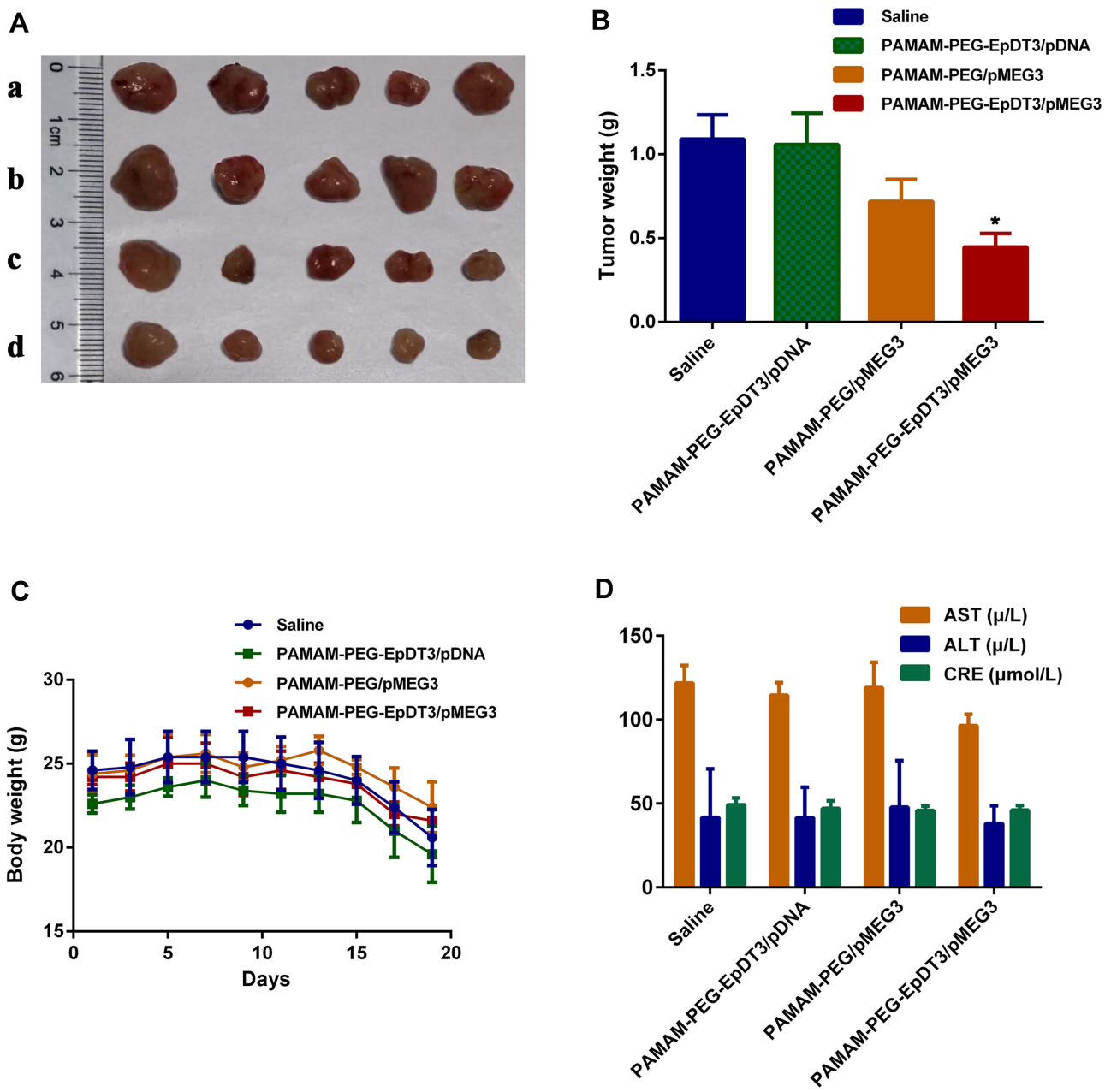

Figure 7 Antitumor effect and safety evaluation in tumor-bearing nude mice. (**A**) Tumors excised upon necropsying castration-resistant prostate cancer (CRPC)-bearing nude mice (a. Saline; b. PAMAM-PEG-EpDT3/pDNA; c. PAMAM-PEG/pMEG3; d. PAMAM-PEG-EpDT3/pMEG3). (**B**) The average weights of the tumors in the different treatment groups (n=5). (**C**) Weights of CRPC-bearing nude mice during the study period (n=5). (**D**) Levels of AST, ALT, and CRE in each treatment group of CRPC-bearing nude mice. *P<0.05 compared to other groups.

Abbreviations: ALT, alanine aminotransferase; AST, aspartate aminotransferase; CRE, creatinine; PAMAM, poly(amidoamine); PEG, polyethylene glycol; pMEG3, plasmid-encoding long non-coding RNA *MEG3*.

results indicate that lncRNA *MEG3* is the primary tumor growth inhibitor in the PAMAM-PEG/pMEG3 and PAMAM-PEG-EpDT3/pMEG3 complexes, and not the nanocarrier itself. Moreover, modifying the EpDT3 aptamer can induce more NP accumulation in the CRPC, improving the efficiency of lncRNA *MEG3* expression in tumors.

Figure 7C shows the average weight changes in nude mice with transplanted tumors in each group. The weights were relatively stable across all groups during the first 13 days; the average weight distribution was 22–25 g. Furthermore, the weights of the nude mice in all groups declined; those in the saline and PAMAM-PEG-EpDT3/pDNA groups decreased significantly to

approximately 19 g. Whereas, the weights of the mice in the PAMAM-PEG/pMEG3 and PAMAM-PEG-EpDT3 /pMEG3 groups decreased less markedly and remained above 20 g. We postulate that the decline in weight in the saline and PAMAM-PEG-EpDT3/pDNA groups during the latter period was caused by the tumor tissues absorbing nutrients from the animals' bodies given the proliferation of tumor blood vessels. However, PAMAM-PEG/pMEG3 and PAMAM-PEG-EpDT3/pMEG3 treatment caused the tumors to be smaller, thereby limiting the weight loss of mice treated with these complexes. Moreover, body weight data also indicated that the nanocarrier itself had no appreciable adverse effects.

To assess the safety of the treatment, we injected the NPs intravenously in healthy mice and collected blood samples 24 h later. As shown in Figure 7D, levels of AST and ALT (two important indicators of liver function), as well as those of CRE (an important indicator of kidney function) did not differ significantly between the groups. This indicated that neither the nanocarriers nor lncRNA-carrying NPs impaired liver and kidney functions in the nude mice; therefore, they are safe gene delivery systems.

Histological Analysis

Figure 8 shows the hematoxylin and eosin staining results of tumor tissues from the nude mice in each drug delivery group. The panels a–d in Figure 8 are saline, PAMAM-PEG -EpDT3/pDNA, PAMAM-PEG/pMEG3 and PAMAM-PEG-EpDT3/pMEG3 groups, respectively. The saline and PAMAM-PEG-EpDT3/pDNA groups showed good tumor growth, no areas of necrosis, large tumor cell nuclei, and relatively clear edges, indicating that the nanocarriers had no obvious toxicities or adverse effects. The PAMAM-PEG /pMEG3 and PAMAM-PEG-EpDT3/pMEG3 groups had loose or vacuolar tumor tissue. Moreover, deep nuclear staining as well as fragmentation and dissolution, accompanied by neutrophil infiltration, was also observed in tissues from PAMAM-PEG-EpDT3/pMEG3-treated mice. These results indicate that lncRNA *MEG3* can inhibit CRPC properties, while the EpDT3 aptamer-modified NPs have an even stronger anti-CRPC effect.

Next, we investigated the mechanism of action of PAMAM-PEG-EpDT3/pMEG3 NPs against CRPC by examining the expression levels of Ki67, Bcl-2, cyclin D1, and p53 proteins in the tumor tissues using immunohistochemistry. Ki67 is a nuclear antigen associated with proliferating cells whose function is closely related to mitosis and is indispensable during cell proliferation; it can be used to identify cells outside the G0 phase of the cell cycle, and its expression levels are used to determine the cellular proliferation index.[36–38] Thus, higher the expression of Ki67, greater the proportion of cells in the proliferation cycle and faster is the rate of tumor growth. The Ki67 protein H-scores in the PAMAM-PEG-EpDT3/pDNA, PAMAM-PEG/pMEG3, and PAMAM-PEG-EpDT3/pMEG3 groups were 54.77, 34.71, and 12.64, respectively; but, the PAMAM-PEG-EpDT3 /pDNA group showed the most intense staining, highest H-score, and maximal expression of Ki67 (Figure 8). Compared to the other groups, the PAMAM-PEG-EpDT3 /pMEG3 group showed superficial staining, low H-score, and low expression of Ki67, indicating that lncRNA *MEG3* significantly inhibits the proliferation in CRPC cells. The EpDT3 aptamer enabled the agents to accumulate at the tumor sites, improving the transfection efficiency of pMEG3 and inhibiting the proliferation of cancer cells.

The Bcl-2 protein is a pro-survival/anti-apoptosis protein.[39–41] As shown in Figure 8, both the saline and PAMAM-PEG-EpDT3/pDNA groups showed intense staining and high positive expression of Bcl-2, while both the PAMAM-PEG/pMEG3 and PAMAM-PEG-EpDT3/pMEG3 groups showed a reduced staining intensity and low expression of Bcl-2, indicating that lncRNA *MEG3* potently promotes apoptosis in CRPC cells.

Cyclin D1 protein was found to be expressed in the tissues of mice from all the drug delivery groups (Figure 8). The saline and PAMAM-PEG-EpDT3/pDNA groups exhibited high cyclin D1 expression, while the PAMAM-PEG-/pMEG3 and PAMAM-PEG-EpDT3/pMEG3 groups showed reduced staining intensities and H-scores. Cyclin D1 is a key protein regulating the G1 phase of the cell cycle; its main function is to promote cell proliferation. It is also a proto-oncogene, and its overexpression leads to uncontrolled cell proliferation and malignancy.[42–44] These results indicate that lncRNA *MEG3* blocks the cell cycle and inhibits proliferation in CRPC cells.

Finally, we investigated the expression of p53 protein in all groups. The wild-type *TP53* is a tumor suppressor that inhibits the proliferation and differentiation in cancer cells and regulates the G1 phase of the cell cycle.[45] When mutated or inactivated, p53 acts as an oncogene and promotes tumorigenesis.[46] The wild-type p53 protein is unstable and has a short half-life, and is therefore difficult to detect via immunohistochemistry. Mutations in the *TP53* are strongly correlated with upregulated p53 expression as determined by immunohistochemistry.[47–49] As shown in Figure 8, the saline group had the highest level of p53,

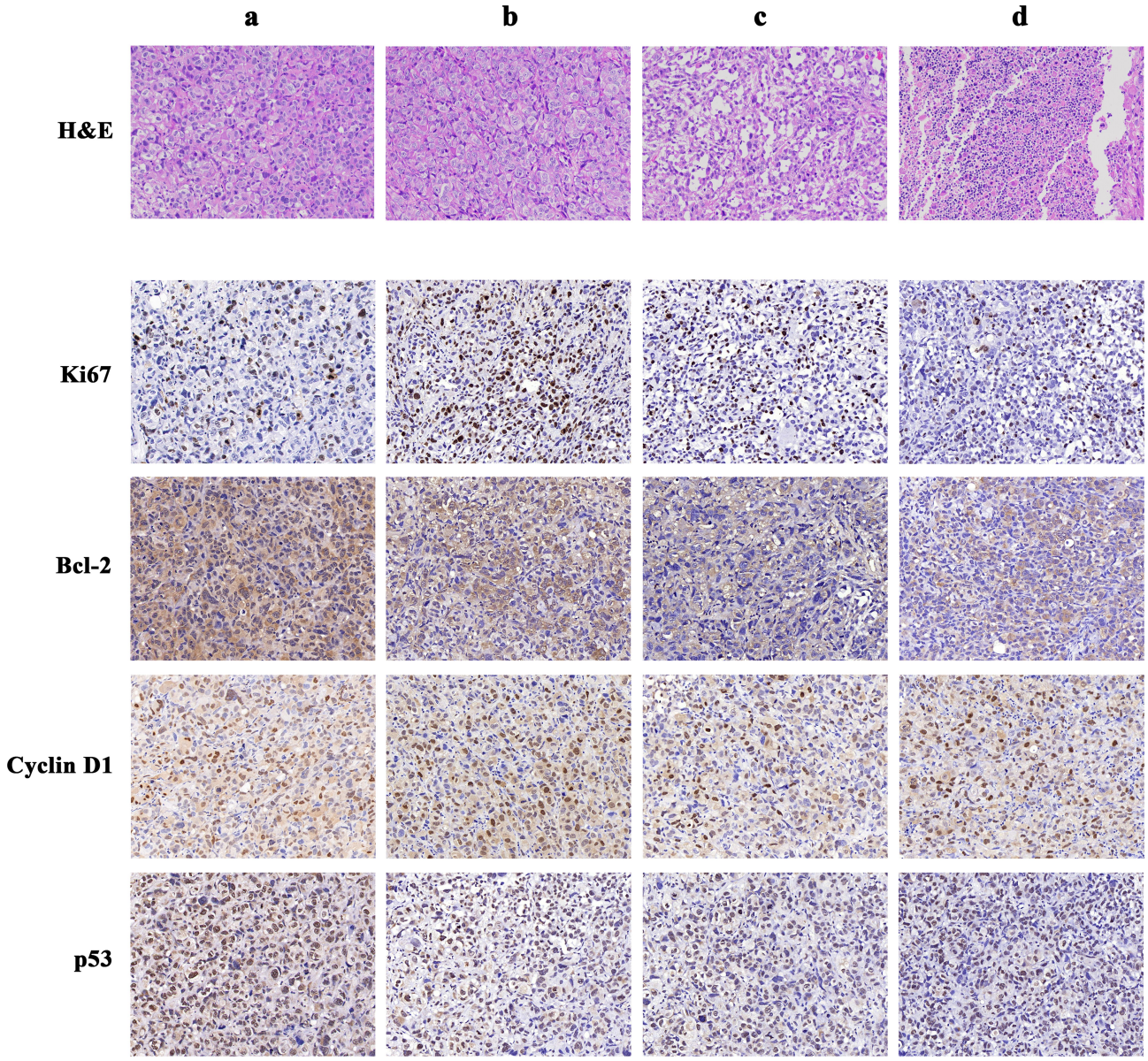

Figure 8 H&E staining of the injured tissue, as well as immunohistochemistry to assess the expression of the indicated proteins in the isolated tumors. (a. Saline; b. PAMAM-PEG-EpDT3/pDNA; c. PAMAM-PEG/pMEG3; d. PAMAM-PEG-EpDT3/pMEG3).
Abbreviations: H&E, hematoxylin and eosin; PAMAM, poly(amidoamine); PEG, polyethylene glycol; pMEG3, plasmid-encoding long non-coding RNA *MEG3*.

followed by the PAMAM-PEG-EpDT3/pDNA, PAMAM-PEG/pMEG3, and PAMAM-PEG-EpDT3/pMEG3 groups. The lower p53 levels in the latter groups indicated that lncRNA*MEG3* significantly inhibited the proliferation in CRPC cells. Compared to the PAMAM-PEG/pMEG3 group, the PAMAM-PEG-EpDT3/pMEG3 group showed relatively shallow staining and had a low H-score. The low positive expression of mutated p53 indicated that lncRNA *MEG3* was transferred to CRPC cells via EpDT3 aptamer targeting, thereby inhibiting cell proliferation.

Conclusion

Based on dendrimers (PAMAM), we developed the PAMAM-PEG-EpDT3 NP as a novel carrier for the targeted delivery of a plasmid-encoding lncRNA MEG3 to CRPC cells. PAMAM-PEG-EpDT3 exhibits excellent CRPC cell targeting capability that is vastly improved over non-EpDT3-modified carriers. PAMAM-PEG-EpDT3 and pMEG3 can form nanoparticles with suitable particle size and potential. Moreover, we elucidated the potential mechanism underlying the cellular uptake of PAMAM-PEG-EpDT3/pMEG3 NPs.

In vitro and in vivo models confirmed the anti-CRPC effect of PAMAM-PEG-EpDT3/pMEG3 NPs, which indicate its great potential as a gene therapy agent for patients with CRPC.

Abbreviations

CRPC, castration-resistant prostate cancer; lncRNA, long non-coding RNA; PAMAM, poly(amidoamine); PEG, polyethylene glycol; NP, nanoparticle; PCa, prostate cancer; N/P ratio, nitrogen-to-phosphorous ratio; pMEG3, plasmid-encoding lncRNA *MEG3*; PBS, phosphate-buffered saline; MAL, maleimide; NHS, N-hydroxysuccinimide; EMA, ethidium monoazide bromide; ^{1}H-NMR, proton nuclear magnetic resonance; ALT, alanine aminotransferase; AST, aspartate aminotransferase; CRE, creatinine.

Ethics Approval

The animal experiments were approved by the ethics committee of Shanghai Skin Disease Hospital. All the animal procedures were performed in accordance with the Guidelines for Care and Use of Laboratory Animals of Tongji University.

Acknowledgments

This work was supported by the National Natural Science Foundation of China (81472394 and 81803078) and the Key Discipline Construction Project and Doctoral Supervisor Candidate of Shanghai Skin Disease Hospital (2019zdxk03, 17HBDS02, and 17HBDS03).

Disclosure

The authors report no conflicts of interest related to this work.

References

1. Eastham JA, Heller G, Halabi S, et al. Cancer and Leukemia Group B 90203 (Alliance): radical prostatectomy with or without neoadjuvant chemohormonal therapy in localized, high-risk prostate cancer. *J Clin Oncol*. 2020;38(26):3042–3050. doi:10.1200/JCO.20.00315
2. Parker C, Castro E, Fizazi K, et al. Prostate cancer: ESMO clinical practice guidelines for diagnosis, treatment and follow-up. *Ann Oncol*. 2020;31:1119–1134. doi:10.1016/j.annonc.2020.06.011
3. Perera M, Roberts MJ, Klotz L, et al. Intermittent versus continuous androgen deprivation therapy for advanced prostate cancer. *Nat Rev Urol*. 2020;17(8):469–481. doi:10.1038/s41585-020-0335-7
4. Gjyrezi A, Xie F, Voznesensky O, et al. Taxane resistance in prostate cancer is mediated by decreased drug-target engagement. *J Clin Invest*. 2020;130(6):3287–3298. doi:10.1172/JCI132184
5. Sternberg CN, Fizazi K, Saad F, et al. Enzalutamide and survival in nonmetastatic, castration-resistant prostate cancer. *N Engl J Med*. 2020;382(23):2197–2206. doi:10.1056/NEJMoa2003892
6. van Haasteren J, Li J, Scheideler OJ, Murthy N, Schaffer DV. The delivery challenge: fulfilling the promise of therapeutic genome editing. *Nat Biotechnol*. 2020;38(7):845–855. doi:10.1038/s41587-020-0565-5
7. Ma CC, Wang ZL, Xu T, He ZY, Wei YQ. The approved gene therapy drugs worldwide: from 1998 to 2019. *Biotechnol Adv*. 2020;40:107502. doi:10.1016/j.biotechadv.2019.107502
8. Wolin SL, Maquat LE. Cellular RNA surveillance in health and disease. *Science (New York, NY)*. 2019;366(6467):822–827. doi:10.1126/science.aax2957
9. Revia RA, Stephen ZR, Zhang M. Theranostic nanoparticles for RNA-based cancer treatment. *Acc Chem Res*. 2019;52(6):1496–1506. doi:10.1021/acs.accounts.9b00101
10. Yao RW, Wang Y, Chen LL. Cellular functions of long noncoding RNAs. *Nat Cell Biol*. 2019;21(5):542–551.
11. Peng W, Si S, Zhang Q, et al. Long non-coding RNA MEG3 functions as a competing endogenous RNA to regulate gastric cancer progression. *J Exp Clin Cancer Res*. 2015;34(1):79. doi:10.1186/s13046-015-0197-7
12. Uroda T, Anastasakou E, Rossi A, et al. Conserved pseudoknots in lncRNA MEG3 are essential for stimulation of the p53 pathway. *Mol Cell*. 2019;75(5):982–995.e989. doi:10.1016/j.molcel.2019.07.025
13. Shihabudeen Haider Ali MS, Cheng X, Moran M, et al. LncRNA Meg3 protects endothelial function by regulating the DNA damage response. *Nucleic Acids Res*. 2019;47(3):1505–1522.
14. Luo G, Wang M, Wu X, et al. Long non-coding RNA MEG3 inhibits cell proliferation and induces apoptosis in prostate cancer. *Cell Physiol Chem*. 2015;37(6):2209–2220. doi:10.1159/000438577
15. Wahlestedt C. Targeting long non-coding RNA to therapeutically upregulate gene expression. *Nat Rev Drug Discov*. 2013;12(6):433–446.
16. Huarte M. The emerging role of lncRNAs in cancer. *Nat Med*. 2015;21(11):1253–1261. doi:10.1038/nm.3981
17. Wu P, Mo Y, Peng M, et al. Emerging role of tumor-related functional peptides encoded by lncRNA and circRNA. *Mol Cancer*. 2020;19(1):22. doi:10.1186/s12943-020-1147-3
18. Maetzel D, Denzel S, Mack B, et al. Nuclear signalling by tumour-associated antigen EpCAM. *Nat Cell Biol*. 2009;11(2):162–171. doi:10.1038/ncb1824
19. Gires O, Pan M, Schinke H, Canis M, Baeuerle PA. Expression and function of epithelial cell adhesion molecule EpCAM: where are we after 40 years? *Cancer Metastasis Rev*. 2020;39(3):969–98. doi:10.1007/s10555-020-09898-3
20. Ni J, Cozzi P, Hao J, et al. Epithelial cell adhesion molecule (EpCAM) is associated with prostate cancer metastasis and chemo/radioresistance via the PI3K/Akt/mTOR signaling pathway. *Int J Biochem Cell Biol*. 2013;45(12):2736–2748. doi:10.1016/j.biocel.2013.09.008
21. Gupta S, Li J, Kemeny G, et al. Whole genomic copy number alterations in circulating tumor cells from men with abiraterone or enzalutamide-resistant metastatic castration-resistant prostate cancer. *Clin Cancer Res*. 2017;23(5):1346–1357. doi:10.1158/1078-0432.CCR-16-1211
22. Ni J, Cozzi PJ, Duan W, et al. Role of the EpCAM (CD326) in prostate cancer metastasis and progression. *Cancer Metastasis Rev*. 2012;31(3–4):779–791. doi:10.1007/s10555-012-9389-1
23. Ptacek J, Zhang D, Qiu L, et al. Structural basis of prostate-specific membrane antigen recognition by the A9g RNA aptamer. *Nucleic Acids Res*. 2020;48:11130–11145. doi:10.1093/nar/gkaa494
24. He XY, Ren XH, Peng Y, et al. Aptamer/peptide-functionalized genome-editing system for effective immune restoration through reversal of PD-L1-mediated cancer immunosuppression. *Adv Mater (Deerfield Beach, Fla)*. 2020;32(17):e2000208. doi:10.1002/adma.202000208
25. Tan W, Li L, Xu S, et al. Nucleic acid aptamers for molecular diagnostics and therapeutics: advances and perspectives. *Angew Chem Int Ed Engl*. 2020. doi:10.1002/anie.202003563

26. Shigdar S, Lin J, Yu Y, Pastuovic M, Wei M, Duan W. RNA aptamer against a cancer stem cell marker epithelial cell adhesion molecule. *Cancer Sci*. 2011;102(5):991–998. doi:10.1111/j.1349-7006.2011.01897.x
27. Xiang D, Shigdar S, Bean AG, et al. Transforming doxorubicin into a cancer stem cell killer via EpCAM aptamer-mediated delivery. *Theranostics*. 2017;7(17):4071–4086. doi:10.7150/thno.20168
28. Wang G, Zhou Z, Zhao Z, et al. Enzyme-triggered transcytosis of dendrimer-drug conjugate for deep penetration into pancreatic tumors. *ACS Nano*. 2020;14(4):4890–4904. doi:10.1021/acsnano.0c00974
29. Li HJ, Liu J, Luo YL, et al. Intratumor performance and therapeutic efficacy of PAMAM dendrimers carried by clustered nanoparticles. *Nano Lett*. 2019;19(12):8947–8955. doi:10.1021/acs.nanolett.9b03913
30. Gong C, Hu C, Gu F, et al. Co-delivery of autophagy inhibitor ATG7 siRNA and docetaxel for breast cancer treatment. *J Control Release*. 2017;266:272–286. doi:10.1016/j.jconrel.2017.09.042
31. Guo X, Wang L, Duval K, Fan J, Zhou S, Chen Z. Dimeric drug polymeric micelles with acid-active tumor targeting and FRET-traceable drug release. *Adv Mater (Deerfield Beach, Fla)*. 2018;30(3). doi:10.1002/adma.201705436
32. Gao F, Tang Y, Liu WL, et al. Intra/extracellular lactic acid exhaustion for synergistic metabolic therapy and immunotherapy of tumors. *Adv Mater (Deerfield Beach, Fla)*. 2019;31(51):e1904639. doi:10.1002/adma.201904639
33. He J, Li C, Ding L, et al. Tumor targeting strategies of smart fluorescent nanoparticles and their applications in cancer diagnosis and treatment. *Adv Mater (Deerfield Beach, Fla)*. 2019;31(40):e1902409. doi:10.1002/adma.201902409
34. Al-Ahmady ZS, Jasim D, Ahmad SS, et al. Selective liposomal transport through blood brain barrier disruption in ischemic stroke reveals two distinct therapeutic opportunities. *ACS Nano*. 2019;13(11):12470–12486. doi:10.1021/acsnano.9b01808
35. Wang T, Zhang J, Hou T, Yin X, Zhang N. Selective targeting of tumor cells and tumor associated macrophages separately by twin-like core-shell nanoparticles for enhanced tumor-localized chemoimmunotherapy. *Nanoscale*. 2019;11(29):13934–13946. doi:10.1039/C9NR03374B
36. Robertson JFR, Coleman RE, Cheung KL, et al. Proliferation and AKT activity biomarker analyses after capivasertib (AZD5363) treatment of patients with ER(+) invasive breast cancer (STAKT). *Clin Cancer Res*. 2020;26(7):1574–1585. doi:10.1158/1078-0432.CCR-19-3053
37. Lawrence MG, Obinata D, Sandhu S, et al. Patient-derived models of abiraterone- and enzalutamide-resistant prostate cancer reveal sensitivity to ribosome-directed therapy. *Eur Urol*. 2018;74(5):562–572. doi:10.1016/j.eururo.2018.06.020
38. Ellis MJ, Suman VJ, Hoog J, et al. Ki67 proliferation index as a tool for chemotherapy decisions during and after neoadjuvant aromatase inhibitor treatment of breast cancer: results from the American College of Surgeons Oncology Group Z1031 trial (Alliance). *J Clin Oncol*. 2017;35(10):1061–1069. doi:10.1200/JCO.2016.69.4406
39. García-Sáez AJ. The BCL-2 family saga. *Nat Rev Mol Cell Biol*. 2020;21:564–565. doi:10.1038/s41580-020-0276-2
40. Delbridge AR, Grabow S, Strasser A, Vaux DL. Thirty years of BCL-2: translating cell death discoveries into novel cancer therapies. *Nat Rev Cancer*. 2016;16(2):99–109. doi:10.1038/nrc.2015.17
41. Ashkenazi A, Fairbrother WJ, Leverson JD, Souers AJ. From basic apoptosis discoveries to advanced selective BCL-2 family inhibitors. *Nat Rev Drug Discov*. 2017;16(4):273–284. doi:10.1038/nrd.2016.253
42. Yu Z, Wang L, Wang C, et al. Cyclin D1 induction of Dicer governs microRNA processing and expression in breast cancer. *Nat Commun*. 2013;4:2812. doi:10.1038/ncomms3812
43. Shan J, Zhao W, Gu W. Suppression of cancer cell growth by promoting cyclin D1 degradation. *Mol Cell*. 2009;36(3):469–476. doi:10.1016/j.molcel.2009.10.018
44. Kim Y, Jin D, Lee BB, et al. Overexpression of β-catenin and cyclin D1 is associated with poor overall survival in patients with stage IA-IIA squamous cell lung cancer irrespective of adjuvant chemotherapy. *J Thorac Oncol*. 2016;11(12):2193–2201. doi:10.1016/j.jtho.2016.07.021
45. Duffy MJ, Synnott NC, O'Grady S, Crown J. Targeting p53 for the treatment of cancer. *Semin Cancer Biol*. 2020. doi:10.1016/j.semcancer.2020.07.005
46. Zhang C, Liu J, Xu D, Zhang T, Hu W, Feng Z. Gain-of-function mutant p53 in cancer progression and therapy. *J Mol Cell Biol*. 2020. doi:10.1093/jmcb/mjaa040
47. Moreira AL, Won HH, McMillan R, et al. Massively parallel sequencing identifies recurrent mutations in TP53 in thymic carcinoma associated with poor prognosis. *J Thorac Oncol*. 2015;10(2):373–380. doi:10.1097/JTO.0000000000000397
48. Dibra D, Mitra A, Newman M, et al. Lack of immunomodulatory interleukin-27 enhances oncogenic properties of mutant p53 in vivo. *Clin Cancer Res*. 2016;22(15):3876–3883. doi:10.1158/1078-0432.CCR-15-2052
49. Yemelyanova A, Vang R, Kshirsagar M, et al. Immunohistochemical staining patterns of p53 can serve as a surrogate marker for TP53 mutations in ovarian carcinoma: an immunohistochemical and nucleotide sequencing analysis. *Modern Pathol*. 2011;24(9):1248–1253. doi:10.1038/modpathol.2011.85